Electronic structure of elemental curium studied by photoemission

T. Gouder,[1] G. van der Laan,[2] A. B. Shick,[3] R. G. Haire,[4] and R. Caciuffo[1]

[1]*European Commission, Joint Research Centre, Institute for Transuranium Elements, Postfach 2340, D-76125 Karlsruhe, Germany*

[2]*Diamond Light Source, Chilton, Didcot OX11 0DE, United Kingdom*

[3]*Institute of Physics, Academy of Sciences of the Czech Republic, Na Slovance 2, CZ-18221 Prague, Czech Republic*

[4]*Oak Ridge National Laboratory, Chemical Science Division, Office Box 2008, MS-6375, Oak Ridge, Tennessee 37831, USA*

(Received 16 December 2010; revised manuscript received 3 February 2011; published 21 March 2011)

The electronic structure of curium metal has been investigated by valence-band and $4f$ core-level photoemission spectroscopy using a high-purity ^{248}Cm sample. The experimental spectra are dominated by poorly screened features and indicate full localization of the $5f$ electrons, in strong contrast to the lighter actinides, including Pu and Am. The results obtained are in good agreement with the Cm photoemission obtained by atomic multielectronic calculations for a $5f^7$ configuration and with the total $5f$ density of states calculated *ab initio* within a correlated band theory model based on the self-consistent, local-density-matrix approximation to the dynamical mean-field theory.

DOI: 10.1103/PhysRevB.83.125111 PACS number(s): 79.60.−i, 71.20.Gj, 71.10.−w

I. INTRODUCTION

Understanding the electronic structure of actinides, the backbone of nuclear energy technology, is an arduous task requiring advances on both theoretical and experimental fronts.[1–4] In transplutonium elements through californium, only $6d$ and $7s$ states are involved in the metallic bonding. Their $5f$ electrons, situated inside the radon core, are localized and do not contribute to the cohesive properties of the solid.[1] Curium, which is in the middle of the actinide series, has a half-filled shell with seven $5f$ electrons. At ambient pressure and room temperature, Cm metal exhibits a double-hexagonal close-packed structure with the space group $P6_3/mmc$.[5] The magnetic susceptibility shows an antiferromagnetic transition at $T_N \approx 65$ K and a Curie-Weiss behavior with an effective paramagnetic moment $\mu_{\text{eff}} \approx 8\ \mu_{\text{B}}$ at higher temperatures.[6] The electrical resistivity behavior is typical for antiferromagnetic metals, with $\varrho \propto T^2$ below T_N and $\varrho \propto T$ above T_N.[7,8] At room temperature, the value of ϱ is close to 100 $\mu\Omega$cm, which is 1–2 orders of magnitude higher than for simple metals, such as K or Al, at the same condition.[8]

A sequence of structural transformations is observed when hydrostatic pressure is applied, including a transition to a monoclinic structure ($C2/c$), found at intermediate pressures between ∼37 and ∼56 GPa, which is stabilized by magnetic correlations of the $5f$ electrons.[5] *Ab initio* electronic structure calculations, allowing for spin polarization of the $5f$ electrons, reproduce the sequence of structures observed during compression and predict ordered magnetic moments at ambient pressure of almost 7 μ_{B},[5] in agreement with experiments.[6,9]

Important information on the electronic structure of actinide elements has been obtained from electron energy-loss spectroscopy (EELS) measurements. The branching ratio of the $N_{4,5}$ ($4d \rightarrow 5f$) absorption edge observed in EELS has been related via a sum rule to the expectation value of the angular part of the $5f$ spin-orbit interaction per hole,[10–12] giving information on the relativistic nature of the $5f$ electrons. EELS results show that the angular momentum coupling is close to the jj limit in the case of Pu and Am but is strongly shifted toward the LS limit in the case of Cm metal. Maximal energy gain in jj coupling is obtained for Am f^6 since the $f_{5/2}$ level is fully filled. However, the f^7 configuration of Cm has a maximal energy stabilization due to exchange interactions, with all spins parallel in the half-filled shell, which can only be achieved in LS coupling. This is reflected in the large change observed in the $N_{4,5}$ branching ratio between Am and Cm. It is the large swing toward LS coupling which produces the strong spin polarization that stabilizes curium.[13] The importance of Hund's rule coupling (i.e., Coulomb interaction) in the stabilization of the curium ground state is confirmed by a study based on the combination of density functional theory in the local-density approximation (LDA) and dynamical mean-field theory, including spin-orbit coupling, itinerancy, and multiplet effects.[14,15] These calculations show that the $5f$ electrons in curium are locked within a single f^7 atomic configuration.

The electronic structure and the valence spectral densities of Cm metal in the paramagnetic phase have also been calculated within the correlated band theory based on LDA + Hubbard-I approximation (HIA), including self-consistency over the charge density, by the full-potential linearized augmented plane-wave (FP-LAPW) method.[16] These calculations provide a self-consistent value for the $5f$ occupation number of $n_f \approx 7$, with ∼3 electrons in the $j = 7/2$ subshell, in agreement with many-electron atomic spectral calculations in intermediate coupling[1] and experimental determinations.[13]

On the other hand, local-spin-density calculations with self-interaction correction predict the occurrence of a mixed-valence state with 6 localized and 1.56 delocalized $5f$ electrons in the paramagnetic case, not in accord with experimental observations, and a more stable antiferromagnetic arrangement with 7 localized and 0.26 bandlike $5f$ electrons.[17]

Here we report the results of valence- and core-state photoemission (PE) spectroscopy measurements performed at room temperature on ^{248}Cm metal. The results are compared with multielectron atomic spectra calculations and with total spectral densities calculated using *ab initio* based correlated band theory.

II. EXPERIMENTAL DETAILS

Photoelectron spectra were recorded using a SPECS Phoibos 100 hemispherical analyzer, with pass energy of 50 eV, 3-mm aperture, and medium amplification. X-ray PE spectra were collected using nonmonochromatized Mg $K\alpha$ (1253.6 eV) radiation with an energy resolution of ~0.7 eV for the Au $4f_{7/2}$ peak. Ultraviolet PE spectra (UPS) were measured using He I, He II, and He II-β excitation ($h\nu = 21.22, 40.81$, and 48.4 eV, respectively) produced by a high-density plasma, UV rare-gas discharge source (SPECS). The total resolution in UPS was 100 meV. The background pressure in the analysis chamber was better than 10^{-8} Pa. All data were corrected for the energy-dependent transmission of the spectrometer.

The ^{248}Cm metal sample used in the experiment was prepared at Oak Ridge National Laboratory by reduction of curium tetrafluoride with lithium metal. The product was arc melted and spat cooled to yield a flat platelet. The sample for the PE studies was shaved from this platelet. A 0.1-mg flake, with a surface area of about 1×1 mm^2, was attached onto a molybdenum wire pin (Ø = 0.1 mm) with silver epoxy glue. The wire was fixed on the sample transfer rod. The surface of the sample was cleaned in situ by Ar ion sputtering (1 keV, 0.1 μA) at room temperature.

III. PHOTOEMISSION RESULTS

A. Cm 4f core-level spectra

The Cm $4f$ core-level spectra obtained before and after Ar ion sputtering are shown in Fig. 1. The spectral range also includes the O $1s$ signal, which for the pristine sample is observed at 530.54- and 532.53-eV binding energy (BE). They reveal the presence of lattice oxygen and surface oxygen and hydroxyl species, respectively. The O $1s$ to Cm $4f$ intensity ratio, corrected for the atomic cross sections, shows that near the surface the initial composition is close to Cm_2O_3, or possibly a somewhat higher oxide. After cleaning, the O $1s$ signal is strongly reduced, meaning that the oxygen contamination of the sample surface became negligible. As the size of the x-ray beam spot is larger than that of the sample,

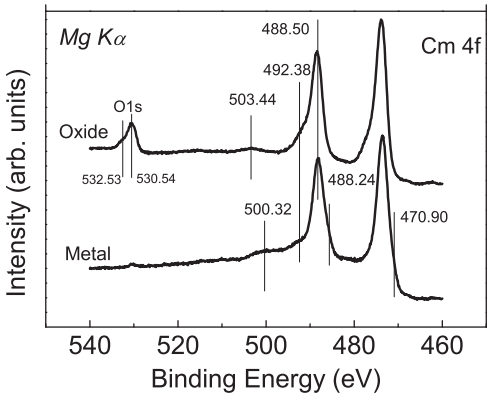

FIG. 1. Cm $4f$ core-level X-ray PE spectra recorded before (upper curve) and after (lower curve) removing surface oxygen contamination by Ar ion sputtering. Vertical bars indicate spectral features affected by the cleaning procedure.

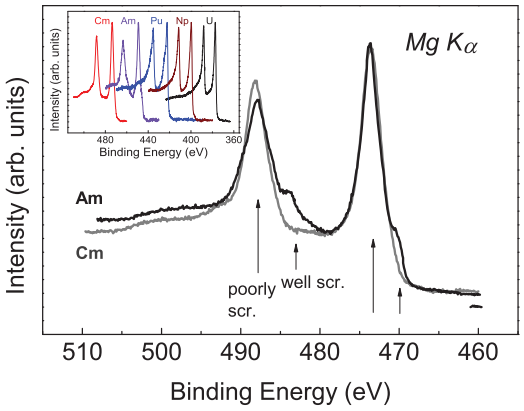

FIG. 2. (Color online) Comparison between the $4f$ PE spectra of Cm (gray curve) and Am (black curve) metal measured with Mg $K\alpha$ radiation. The Am spectrum has been shifted in BE to overlap with the Cm one. Vertical arrows indicate well-screened and poorly screened final states in the Am spectrum. Only poorly screened features are visible for Cm. The inset shows the $4f$ PE spectra of U, Np, Pu, Am, and Cm.

the weak residual O $1s$ signal is most probably associated with the sample holder. In the He I spectra, collected with a source having a small focal spot and irradiating only the sample surface, no oxygen is observed, and the O $2p$ line is consequently missing (See Sec. III B).

The removal of the oxide surface layer also modified the shape of the spin-orbit split Cm $4f$ signal, represented by the two strong $4f_{5/2}$ and $4f_{7/2}$ PE peaks at 488.24- and 473.62-eV BE, respectively. In the case of the oxygen-contaminated surface, the $4f_{5/2}$ peak has a shoulder at 3.88-eV higher BE, whereas for the cleaned metal a shoulder was observed at 2.53-eV lower BE. These changes reflect the variation in exchange interaction between the $4f$ core hole and the localized $5f$ shell in the metal ($5f^7$ configuration) and in higher oxide ($5f^6$ configuration). The $4f$ spin-orbit splitting (14.62 eV) is not substantially affected, but the doublet structure is shifted by −0.26 eV. This shift is close to that observed in Am[18] but significantly smaller than for Pu, Np, or U. The main reason for the shift in the light actinides is that upon oxidation the $5f$ electrons become localized. In the heavier actinides from Am onward the $5f$ states are localized even in the metal. Therefore, the shift upon oxidation is much smaller. The weak and broad feature at 500.32 eV (503.44 eV in the oxide) is probably intrinsic. Its intensity (~2% of the Cm $4f$ peak) is too large to be ascribed to a ghost Mo $3s$ peak (506.3-eV BE; cross section ~2.6% of the Cm $4f$ peak[19]), taking into account that the surface of the Mo wire pin was about 2 orders of magnitude smaller than that of the sample. A similar feature was also observed for americium (see Fig. 2) and was interpreted as a plasmon loss.[18]

The Cm $4f$ PE spectrum is compared to the reported spectrum for Am metal in Fig. 2. The Am spectrum has been shifted to higher BE to superpose onto the Cm. In Am metal, the main lines are accompanied by a satellite at 3-eV lower BE, indicating different final-state screening effects.[18] The low-BE satellite corresponds to the well ($5f$) screened final state, whereas the main peak corresponds to the poorly ($6d$) screened final state. In itinerant $5f$ systems, the well-screened

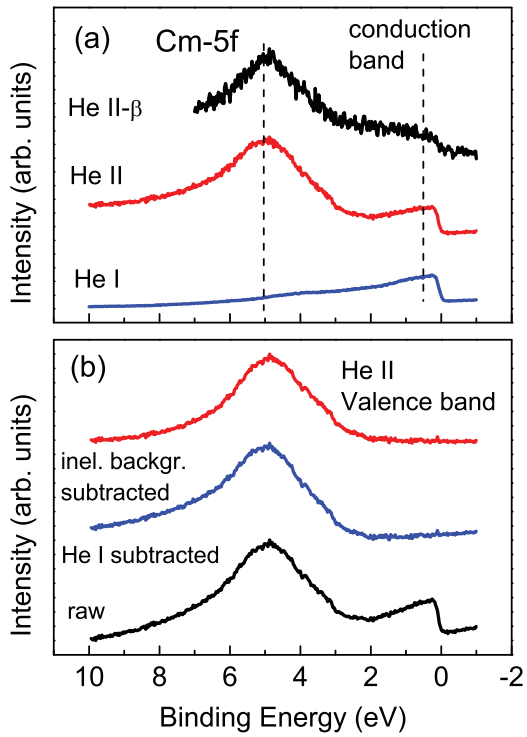

FIG. 3. (Color online) (a) Cm valence-band PE spectra measured with He I, He II, and He II-β radiation. The $5f$ contribution dominates the He II and II-β spectra, while the He I spectrum is dominated by the $6d$ signal. (b) The $5f$ contribution to the Cm valence-band PE spectrum obtained by subtracting the He I spectrum and the inelastic background from the measured He II spectrum.

peak dominates (see U, Np, and Pu $4f$ PE spectra in the inset of Fig. 2), whereas in localized systems the poorly screened peak is strong.[20] The predominance of the poorly screened peak in Am, therefore, exemplifies $5f$ localization, but the still-observable well-screened peak indicates a nonvanishing hybridization of the $5f$ states with the conduction band. In the case of Cm, the absence of the well-screened peak indicates full localization of the $5f$ states.

B. Valence-band spectra

Valence-band PE spectra were measured with He I, He II, and He II-β radiation, and the results are shown in Fig. 3(a). For He I, the spectrum is dominated by the $6d$ electrons. The PE cross section at this photon energy is ~6 times larger than for the $5f$ and 50 times larger than for the $7s$ electrons. While the cross sections of the $6d$ and $7s$ rapidly diminish with increasing photon energy, that of the $5f$ increases, so that the $5f$ to $6d$ cross section ratio increases from ~0.16 (He I) to 10 (He II) to ~33 (He II-β).[19] Hence, the broad peak at 5-eV BE can be attributed to the $5f$ state. It is almost absent in the He I spectra, whereas it becomes the dominant peak in the He II and is almost the only peak in the He II-β spectra. Cm shows only a single broad $5f$ peak, in contrast to Am, which shows two separated $5f$ peaks, attributed to well- and poorly screened final states, just as in the case of the $4f$ core levels. The absence of the well-screened peak in Cm confirms the fully localized character of the $5f$ electrons. The flat signal between 3-eV BE and the Fermi level is attributed to the $6d7s$ conduction band. The intensity rise of the signal with decreasing BE in the He I and He II spectra is due to inelastic background effects.

It should be noted that the absence of any features at 5-eV BE in the He I spectrum is a further indication that the oxygen contamination of the examined surface is extremely small. In fact, the O $2p$ signal, which is also at 5-eV BE, has a very large cross section for He I and would otherwise be dominating the measured spectrum.

The $5f$ contribution to the PE can be isolated to good approximation by subtracting the He I from the He II spectrum (eliminating the conduction-band contribution) and then subtracting the inelastic background by using the Shirley algorithm.[21] The results of this procedure are presented in Fig. 3(b).

IV. MULTIELECTRON ATOMIC SPECTRAL CALCULATIONS

In sharp contrast to the lighter actinides,[20] the case of Cm metal can be described to good approximation by a single $5f^n$ configuration.[16] The ground-state electronic configuration of the Cm atom is $[\mathrm{Rn}]5f^7 6d^1 7(sp)^2$. Since the interaction of the $5f$ electrons within the shell and with other shells is much larger than that of the $6d$ and $7sp$ electrons, we can neglect the latter in the atomic calculation. Inclusion of $6d$ states in the calculation did not substantially alter the spectra, but it would complicate the multiplet assignment in the analysis below. Using the Hartree-Fock scheme of Cowan[22] in intermediate coupling approximation, we obtain the Cm $5f^7$ ground state as 79.8% $^8S_{7/2}$, spin-orbit interaction mixing in 17.3% $^6P_{7/2}$ and 1.9% $^4D_{7/2}$.

The valence $5f$ and core $4f$ PE spectra are obtained by taking into account the transitions to all states of the configurations $5f^6\varepsilon$ and $4f^{13}5f^7\varepsilon$, respectively, where ε is a continuum electron. The electrostatic and spin-orbit interactions of the continuum electron are taken equal to zero. The Hartree-Fock values of the Slater and spin-orbit parameters for the initial and final states are listed in Table I. The Slater integrals were reduced to 70%, as is usual for these calculations in order to account for the effects of intra-atomic correlation, while the spin-orbit parameters were kept at their full strength.[23]

The calculated $5f$ PE due to the transition Cm $5f^7 \rightarrow 5f^6\varepsilon$ is shown in Fig. 4(a). The final state can be approximately described using LS-coupled states as $^7F_{J'}$ with the values of the total angular momentum $J' = L' + S' = 0,1,2,3,4,5,6$. We use the conventional notation that L,S,J, and L',S',J' indicate the total orbital, spin, and angular quantum numbers of the initial and final states, respectively. The line spectrum is shown in Fig. 4. The level of lowest BE is $J' = 0$, where spin and orbit are coupled antiparallel. The intensities of the lines are close to their multiplicity $2J' + 1$. The energy separation between the J' levels is determined by the $F^k(5f,5f)$ Coulomb interaction. The substantial spin-orbit interaction $\zeta(5f)$ gives rise to additional structure at higher BE. Such structure is absent in the PE of Gd $4f^7$ [see Fig. 1(g) in Ref. 24] since the spin-orbit interaction of Gd $4f$ is only about half as large as that of Cm $5f$.

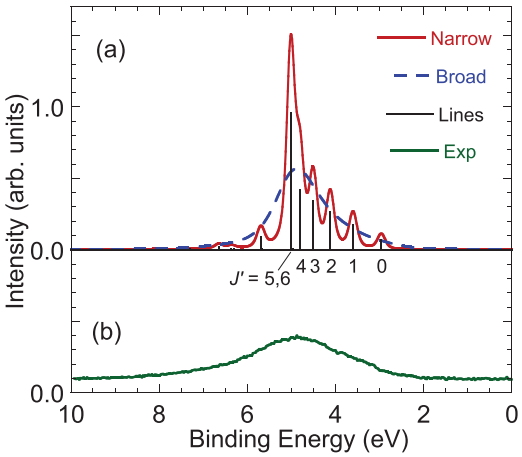

FIG. 4. (Color online) (a) Calculated line intensities and broadened spectra for Cm $5f$ photoemission. The narrow line spectrum is convoluted by a Lorentzian of full width at half maximum $\Gamma = 0.06$ eV and a Gaussian of width $\sigma = 0.06$ eV. The broad line spectrum is convoluted by a Lorentzian of $\Gamma = 0.2$ eV and a Gaussian of $\sigma = 0.3$ eV. (b) Experimental valence PE after background correction measured with He II radiation.

Figure 4(b) shows the experimental $5f$ PE spectrum after background corrections. The agreement is especially good, and although the energy resolution is not sufficient to resolve the individual components, the asymmetric shape of the peak and the extra intensity around 4-eV BE are indicative of the multiplet structure.

The $4f$ PE due to the transition Cm $5f^7 \rightarrow 4f^{13}5f^7\varepsilon$ is shown in Fig. 5. Because of the strong core-hole spin-orbit interaction, the spectral shape can be largely understood in the limit of jj coupling. The $4f$ level splits into $j = 7/2$ and $5/2$ states with an energy separation of $\frac{7}{2}\zeta(4f) \approx 14$ eV, in good agreement with the experimental value of 14.62 eV.

In the final state, the $j = 7/2$ hole of the $4f$ shell couples to the $J = 7/2$ of the $5f^7$ shell, forming a manifold that contains $J' = 0,1,2,3,4,5,6,7$ with multiplicities $2J' + 1$. The energy separation between the J' levels is a measure of the exchange

TABLE I. Atomic Hartree-Fock values of the Slater integrals F^k and G^k and the spin-orbit parameters ζ in eV for the initial- and final-state configurations in the Cm $5f^7 \rightarrow 5f^6\varepsilon$ and Cm $5f^7 \rightarrow 4f^{13}5f^7\varepsilon$ photoemission process, calculated using Cowan's code.

	Cm $5f^7$	Cm $5f^6\varepsilon$	Cm $4f^{13}5f^7\varepsilon$
$F^2(5f,5f)$	10.456	10.990	11.365
$F^4(5f,5f)$	6.825	7.216	7.474
$F^6(5f,5f)$	5.008	5.310	5.505
$\zeta(5f)$	0.386	0.414	0.451
$\zeta(4f)$			4.044
$F^2(4f,5f)$			6.328
$F^4(4f,5f)$			2.800
$F^6(4f,5f)$			1.740
$G^0(4f,5f)$			1.670
$G^2(4f,5f)$			2.119
$G^4(4f,5f)$			1.665
$G^6(4f,5f)$			1.306

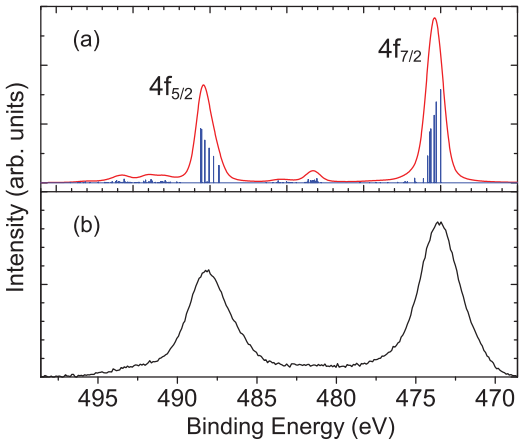

FIG. 5. (Color online) (a) Calculated line intensities and broadened spectrum for Cm $4f$ photoemission. The spectrum is convoluted by a Lorentzian of full width at half maximum $\Gamma = 0.2$ eV and a Gaussian of width $\sigma = 0.3$ eV. (b) Experimental $4f$ PE spectrum after background correction.

interaction. For the $4f_{7/2}$ core hole, spin and orbit are coupled parallel by the spin-orbit interaction, and the $4f$ and $5f$ spins are coupled parallel by the $4f$-$5f$ exchange interaction. This means that in the $4f_{7/2}$ structure $J' = 7$ has the lowest BE.

The $j = 5/2$ hole of the $4f$ shell couples to the $J = 7/2$ of the $5f$ shell, forming a manifold that contains $J' = 6,5,4,3,2,1$. For the $4f_{5/2}$ core hole, the spin and orbit are coupled antiparallel. $J' = 1$, where the spins of the $5f$ and $4f$ are coupled parallel to each other but antiparallel to the $4f$ orbit, has the lowest binding energy. Thus, the ordering in energy of the J' levels in the $4f_{5/2}$ is opposite to that of the $4f_{7/2}$ structure. Hence, the asymmetries of the $4f_{5/2}$ and $4f_{7/2}$ peaks are also opposite (cf. Fig. 5).

As the electrostatic interactions cannot be neglected with respect to the $4f$ spin-orbit interaction, the real situation is not fully described by jj coupling. The calculations, done in intermediate coupling, clearly show these differences in Figs. 4 and 5. The electrostatic interactions give that the distribution over J' levels is only approximate and lead to additional structure outside the main $4f_{7/2}$ and $4f_{5/2}$ manifolds.

The overall agreement between calculated and experimental core-level spectra [Fig. 5(b)] is very good. The predicted asymmetries of the $4f_{5/2}$ and $4f_{7/2}$ lines are confirmed by the experiment. The two weak PE lines centered at +4- and +6-eV higher BE with the respect to the $4f_{5/2}$ main peak would correspond to the shoulder observed at ~492-eV BE. The feature at about +8-eV higher BE from the $4f_{7/2}$ is not observed, probably because it falls on the valley of the experimental spectrum.

V. LDMA CALCULATIONS

In this section we employ the so-called local-density-matrix approximation (LDMA)[16] to the dynamical mean-field theory, which combines the HIA with the FP-LAPW method and includes full self-consistency over the charge density.

In the LDMA, the occupation matrix,

$$n_{\gamma_1\gamma_2} = -\frac{1}{\pi}\,\mathrm{Im}\int_{-\infty}^{E_F} \mathrm{d}z\,[G(z)]_{\gamma_1\gamma_2}, \tag{1}$$

represented in a local basis $\{\phi_\gamma\}$ is self-consistently evaluated with the aid of the local Green's function $G(z)$,

$$[G(z)]^{-1}_{\gamma_1\gamma_2} = [G_{\mathrm{LDA}}(z)]^{-1}_{\gamma_1\gamma_2} - \Delta\epsilon\,\delta_{\gamma_1\gamma_2} - [\Sigma_{\mathrm{H}}(z)]_{\gamma_1\gamma_2}, \tag{2}$$

where $\Sigma_{\mathrm{H}}(z)$ is the HIA self-energy, $\Delta\epsilon$ accounts for the difference between the impurity and the lattice chemical potentials, and $G_{\mathrm{LDA}}(z)$ is the LDA Green's function,

$$[G_{\mathrm{LDA}}(z)]_{\gamma_1\gamma_2} = \frac{1}{V_{\mathrm{BZ}}}\int_{\mathrm{BZ}} d^3k\,[z+\mu - H_{\mathrm{LDA}}(\mathbf{k})]^{-1}_{\gamma_1\gamma_2}. \tag{3}$$

The local-density matrix $n_{\gamma_1\gamma_2}$ is used to construct an effective LDA + U potential V_U, which is inserted into Kohn-Sham-like equations,

$$[-\nabla^2 + V_{\mathrm{LDA}}(\mathbf{r}) + V_U + \xi(\mathbf{l}\cdot\mathbf{s})]\Phi^b_{\mathbf{k}}(\mathbf{r}) = \epsilon^b_{\mathbf{k}}\Phi^b_{\mathbf{k}}(\mathbf{r}). \tag{4}$$

These equations are iteratively solved until self-consistency over the charge density is reached. The new Green's function $G_{\mathrm{LDA}}(z)$ in Eq. (3) and the self-energy $\Sigma_{\mathrm{H}}(z)$ for the new value of the f-shell occupation, obtained from the solution of Eq. (4), are evaluated. The self-consistency loop is closed by inserting the new $G_{\mathrm{LDA}}(z)$ and $\Sigma_{\mathrm{H}}(z)$ into the matrix in Eq. (2) and evaluating the new local occupation matrix $n_{\gamma_1\gamma_2}$ in Eq. (1). At the end, the imaginary part of the local Green's function $G(z)$ in Eq. (2) provides a means to estimate valence-band photoemission spectra.

The LDMA extends the LDA + U approximation in several important aspects. It goes beyond the single Slater determinantal wave functions for the description of the intra-atomic processes and thus inherently incorporates the intermediate coupling regime and accounts for multiplet transitions within the f shell.

Similar to Ref. 16, the calculations were carried out assuming a paramagnetic state with fcc crystal structure and the experimental value of the volume per atom. The Slater integrals were chosen as follows: $U = F_0 = 4.5$ eV, and F_2, F_4, and F_6 were taken as 70% of the calculated Hartree-Fock values in Table I. This choice of Slater integrals corresponds to the exchange $J = 0.61$ eV. The Green's function and self-energy in Eq. (2) were calculated along the real axis $z = \mathrm{Re}\,z + i\delta$ with $\delta = 0.0314$ eV. The inverse temperature $\beta = 40$ eV^{-1} was used, which corresponds to room temperature. For self-consistency, 256 special k points[25] in the irreducible 1/8 part of the BZ were used. The sphere radius $R_{\mathrm{MT}} = 3.1$ a.u. was used, and $R_{\mathrm{MT}} \times K_{\mathrm{max}} = 10.85$ determined the basis-set size. The f-manifold occupation n_f is varied in the calculations until a convergence better than 0.01 for n_f and 0.001 for all components of the on-site occupation matrix $n_{\gamma_1\gamma_2}$ is achieved. The charge density is fully converged to better than 10^{-5} e/a.u.^{3} at each iteration.

Figure 6 shows the total and f-projected densities of states (DOS) resulting from the self-consistent LDMA calculations. Figure 6(a) shows the f-projected DOS (f-DOS) together with its $j = 5/2$ and $j = 7/2$ components. Figure 6(b) shows the total DOS per unit cell (including f and non-f states) and f-DOS.

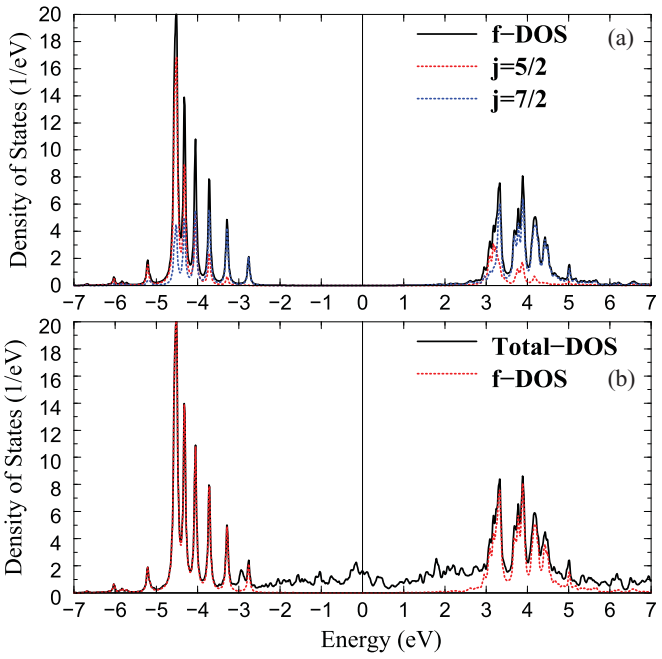

FIG. 6. (Color online) Density of states (DOS) for Cm metal in the self-consistent LDMA approximation, calculated for room temperature [$\beta = (k_B T)^{-1} = 40$ eV^{-1}] as a function of energy (BE changed by sign) measured from the Fermi level. (a) Total and spin-orbit resolved f-DOS. The Coulomb interaction causes a strong admixture of the high-energy $j = 7/2$ and low-energy $j = 5/2$ states. (b) Total DOS and f-DOS.

The self-consistent LDMA values of $n_f = 7.05$, $n_{5/2} = 4.20$, and $n_{7/2} = 2.85$ equate to a $N_{4,5}$ branching ratio $B = 0.76$, which is in reasonable agreement with the experimental value of 0.79.[13] We can estimate the effective local moment by calculating the expectation values of total, spin, and orbital moment operators, **J**, **S**, and **L**. Further, the spin S, orbital L, and total J moment "quantum numbers" are found using $\langle \mathbf{X}^2\rangle = X(X+1)$ for $X = S, L, J$, and the effective magnetic moment $\mu_{\mathrm{eff}} = g_J\sqrt{J(J+1)}$ is evaluated, where the g factor $g_J = (2S+L)/J$ is used. For Cm at room temperature, $S = 3.23$, $L = 0.53$, and $J = 3.50$ are calculated. The corresponding local magnetic moment $\mu_{\mathrm{eff}} = 7.925$ μ_{B} agrees well with the experimental data.[9]

VI. DISCUSSION AND CONCLUSIONS

The room-temperature PE spectra of elemental curium confirm the localized nature of the $5f$ electrons in this metal. Both the $4f$ core-level and the valence-band spectra are dominated by well-screened features, suggesting a fully localized $5f$ configuration. The experimental Cm $5f$ PE is in good agreement with both the total $5f$-DOS calculated by self-consistent LDMA and the Cm $5f$ photoemission obtained by atomic multielectronic calculations for a $5f^7$ configuration. This means that the hybridization (mixing) between the $5f$ configurations is small and supports the conclusion of self-consistent LDMA calculations giving an occupation of the $5f$ manifold very close to 7. The asymmetric shape of the valence-band spectrum is reproduced by both

theoretical models, and the LDMA calculations also give a good description of the conduction band contribution. The presence of a pseudogap around 1-eV BE, suggested in Ref. 14, is not confirmed by the experiment.

The calculated manifold structure of the $5f$-DOS shows distinct J levels, where the energy separation, and hence admixture, is determined by the $F^k(5f,5f)$ Coulomb interactions. The total angular momentum levels at higher BE have larger J values and predominantly $j = 7/2$ character, whereas those at lower BE have lower J values and predominantly $j = 5/2$ character. The experimental Cm $5f$ valence-band PE is in agreement with the broadened calculated $5f$ manifold and shows the absence of other pronounced structure that might otherwise be present due to hybridization.

In both theoretical models, the Slater integrals have been scaled to 70% of their Hartree-Fock values, instead of the default 80% scaling. This choice gives a better agreement for the expectation value of the $5f$ spin-orbit interaction per hole with the value deduced from the $N_{4,5}$ branching ratio B, that has been experimentally obtained using EELS. For an 80% and 70% scaling of the Slater integrals the calculation gives $B = 0.74$ and 0.76, respectively, which can be compared to the experimental value of $B = 0.79$ (Ref. 13). The self-consistency in the LDMA calculation gives an f occupation of $n_f = 7.05$ with occupation numbers for the $j = 5/2$ and $j = 7/2$ subshells of $n_{5/2} = 4.20$ and $n_{7/2} = 2.85$, which is close to the intermediate coupling results.

The peak structure of the $4f$ core-level PE can be used to track the degree of $5f$ localization in the actinides. The experimental Cm $4f$ PE, which shows a spin-orbit split doublet with an energy separation of $\sim$14 eV, is in good agreement with the atomic multielectronic calculations in intermediate coupling for an $5f^7$ ground state. The clear absence of any satellite peaks provides a firm confirmation for the localized nature of the $5f$ ground state in Cm metal. The $4f$ peak structure is very different from those of the lighter actinides, including δ-Pu and Am, where the electronic structure has to be described by (partly) delocalized $5f$ states.

ACKNOWLEDGMENTS

We are grateful to Frank Huber for his help during the experiment. A.B.S. acknowledges the financial support from Czech Republic Grants No. GACR P204/10/0330 and No. AV0Z10100520. The Department of Energy Office of Basic Energy Sciences is thanked for sponsorship of R.G.H.

[1] K. T. Moore and G. van der Laan, Rev. Mod. Phys. **81**, 235 (2009).
[2] P. Santini, S. Carretta, G. Amoretti, R. Caciuffo, N. Magnani, and G. H. Lander, Rev. Mod. Phys. **81**, 807 (2009).
[3] R. Caciuffo, G. van der Laan, L. Simonelli, T. Vitova, C. Mazzoli, M. A. Denecke, and G. H. Lander, Phys. Rev. B **81**, 195104 (2010).
[4] S. Heathman, J.-P. Rueff, L. Simonelli, M. A. Denecke, J.-C. Griveau, R. Caciuffo, and G. H. Lander, Phys. Rev. B **82**, 201103 (2010).
[5] S. Heathman, R. G. Haire, T. Le Bihan, A. Lindbaum, M. Idiri, P. Normile, S. Li, R. Ahuja, B. Johansson, and G. H. Lander, Science **309**, 110 (2005).
[6] P. G. Huray, S. E. Nave, J. R. Peterson, and R. G. Haire, Phys. B + C **102**, 217 (1980).
[7] Y. Y. Tsiovkin, M. A. Korotin, A. O. Shorikov, V. I. Anisimov, A. N. Voloshinskii, A. V. Lukoyanov, E. S. Koneva, A. A. Povzner, and M. A. Surin, Phys. Rev. B **76**, 075119 (2007).
[8] R. Schenkel, Solid State Commun. **23**, 389 (1977).
[9] P. G. Huray and S. E. Nave, *Handbook on the Physics and Chemistry of the Actinides* (North-Holland, Amsterdam, 1987), Vol. 5, p. 311.
[10] B. T. Thole and G. van der Laan, Phys. Rev. B **38**, 3158 (1988).
[11] G. van der Laan, K. T. Moore, J. G. Tobin, B. W. Chung, M. A. Wall, and A. J. Schwartz, Phys. Rev. Lett. **93**, 097401 (2004).
[12] G. van der Laan and B. T. Thole, Phys. Rev. B **53**, 14458 (1996).
[13] K. T. Moore, G. van der Laan, R. G. Haire, M. A. Wall, A. J. Schwartz, and P. Söderlind, Phys. Rev. Lett. **98**, 236402 (2007).
[14] J. H. Shim, K. Haule, and G. Kotliar, Nature (London) **446**, 513 (2007).
[15] J. H. Shim, K. Haule, and G. Kotliar, Europhys. Lett. **85**, 17007 (2009).
[16] A. B. Shick, J. Kolorenč, A. I. Lichtenstein, and L. Havela, Phys. Rev. B **80**, 085106 (2009).
[17] A. Svane, L. Petit, Z. Szotek, and W. M. Temmerman, Phys. Rev. B **76**, 115116 (2007).
[18] T. Gouder, P. M. Oppeneer, F. Huber, F. Wastin, and J. Rebizant, Phys. Rev. B **72**, 115122 (2005).
[19] J. J. Yeh and I. Lindau, At. Data Nucl. Data Tables **32**, 1 (1985).
[20] G. van der Laan and M. Taguchi, Phys. Rev. B **82**, 045114 (2010).
[21] D. A. Shirley, Phys. Rev. B **5**, 4709 (1972).
[22] R. D. Cowan, *Theory of Atomic Structure and Spectra* (University of California Press, Berkeley, 1981).
[23] G. van der Laan and B. T. Thole, Phys. Rev. B **43**, 13401 (1991).
[24] G. van der Laan and B. T. Thole, Phys. Rev. B **48**, 210 (1993).
[25] H. J. Monkhorst and J. D. Pack, Phys. Rev. B **13**, 5188 (1976).